Solar Physics (2025) 300:173
https://doi.org/10.1007/s11207-025-02572-3

RESEARCH

Modeling Decadal and Centennial Solar UV Irradiance Changes

Raffaele Reda[1] · Valentina Penza[1] · Serena Criscuoli[2] · Luca Bertello[2] · Matteo Cantoresi[1] · Lorenza Lucaferri[1] · Simone Ulzega[3] · Francesco Berrilli[1]

Received: 17 June 2025 / Accepted: 25 October 2025 / Published online: 4 December 2025

Abstract
Reconstructions of solar spectral irradiance—especially in the ultraviolet (UV) range—are crucial for understanding Earth's climate system. Although total solar irradiance (TSI) has been thoroughly investigated, the spectral composition of solar radiation offers a deeper insight into its interactions with the atmosphere, biosphere, and climate. UV radiation, in particular, plays a key role in stratospheric chemistry and the dynamics of stratospheric ozone. Reconstructing solar irradiance over the past centuries requires accounting for both the cyclic modulation of active-region coverage associated with the 11-year solar cycle and the longer-term secular trends, including their centennial variability. This study utilizes an empirical framework, based on a 1000-year record of open solar flux, to characterize the various temporal components of solar irradiance variability. We then combine these components to reconstruct solar UV irradiance variations in spectral bands crucial for Earth's atmospheric studies.

Keywords Solar irradiance · Spectrum · Ultraviolet · Solar cycle

1. Introduction

Solar irradiance constitutes the principal energy source for the Earth system, engaging in complex interactions with the terrestrial atmosphere and exerting an influence on climate over long timescales. Extensive efforts have been dedicated to studying total solar irradiance (TSI)—the Sun's irradiance integrated across the entire wavelength spectrum—using both observations and models. However, specific spectral bands — particularly in the ultraviolet (UV) — are critically important across a range of disciplines, including solar and stellar physics, atmospheric modeling, climatology, and the study of habitability conditions on exoplanets (see, e.g., Pienitz and Vincent 2000; Linsky 2014; Lovric et al. 2017; Galuzzo et al. 2021; Reda et al. 2023).

The TSI exhibits typical variations of about 0.1% from minimum to maximum of the 11-year cycle (e.g. Kopp et al. 2016), whereas variations in more energetic spectral bands, such as the UV, can be significantly larger, reaching up to 10% (Fröhlich and Lean 2004; Criscuoli 2019; Woods and DeLand 2021). These variations are particularly important because of the strong interaction of solar radiation at these wavelengths with Earth's upper and middle atmosphere. According to conventional nomenclature, it is possible to divide the UV band

Extended author information available on the last page of the article

into several regions: middle UV (MUV, 180 – 300 nm), far UV (FUV, 115 – 180 nm) and extreme UV (EUV, 10 – 115 nm). Slightly different definitions of these bands, particularly MUV and FUV, can be found in the literature. In this work, we use the definitions adopted by the SOlar Stellar Irradiance Comparison Experiment (SOLSTICE) launched as part of the Solar Radiation and Climate Experiment (SORCE), for which MUV and FUV data are available (McClintock, Snow, and Woods 2005).[1]

In particular, EUV radiation can affect ionospheric and thermospheric structures, and thereby influence, for example, the propagation of radio signals (e.g. Bigazzi, Cauli, and Berrilli 2020). UV radiation also plays a key role in atmospheric density modeling and forecasting, directly influencing satellite orbits due to increased atmospheric drag. In the case of the stratosphere, radiation in the FUV and MUV bands can change ozone levels. In particular, ozone formation is primarily driven by high-energy UV photons with wavelengths shorter than 240 nm, falling within the Schumann-Runge bands and Herzberg continuum. These photons dissociate molecular oxygen O_2, enabling the subsequent creation of ozone O_3 through the reaction between O_2 and atomic oxygen O. Conversely, ozone molecules can be broken apart by lower-energy UV radiation, particularly at wavelengths up to 320 nm (Hartley-Huggins bands). However, this is not the main pathway by which stratospheric ozone is destroyed, because O_2 can easily recombine with O. Additional chemical processes acting at different altitudes – potentially involving catalytic reaction cycles – take part in the radiative interplay that governs the vertical distribution of ozone and its role in stratospheric heating and chemical feedbacks (Chapman 1930; Haigh 2007). Due to the aforementioned mechanisms, the greater variability of the solar cycle in the UV part of the spectrum has a stronger modulating effect on ozone production than on its destruction. This results in a 2 – 4% increase in ozone abundance in the upper stratosphere during periods of solar maximum (Lilensten and Tourpali 2015).

The FUV and MUV bands also enable the calculation of the spectral color index FUV-MUV. This descriptor, introduced by Lovric et al. (2017) and further investigated by Criscuoli et al. (2018), can be used to characterize stellar UV emission and shows a strong correlation with the Mg II index.

This underscores the importance of direct observations for studying solar UV variations. However, systematic measurements of solar UV radiation have only been performed since the advent of space-based telescopes in the late 1960 s, with missions such as the Orbiting Solar Observatory (OSO) 1 (Neupert 1965), Nimbus 7 (Cebula, Park, and Heath 1988), SORCE (McClintock, Snow, and Woods 2005), and the Total and Spectral Solar Irradiance Sensor (TSIS) (Richard et al. 2024). Therefore, reconstructions based on solar and terrestrial proxies are particularly valuable for investigating solar variability in the past centuries (Kakuwa and Satoru 2022).

It is commonly accepted that total solar irradiance and spectral solar irradiance in the visible and near-infrared variations on short to medium timescales, from days to decades, are primarily driven by the presence of dark (sunspots) and bright (network and plage) regions on the solar surface, modulated by the 11-year solar cycle (e.g. Steinegger, Brandt, and Haupt 1996; Berrilli et al. 1999; Ermolli, Berrilli, and Florio 2003; Criscuoli et al. 2023; Marchenko et al. 2024). On longer, secular timescales, variations are also evident, as demonstrated by grand minima and maxima observed in sunspot records and magnetic activity proxies such as radionuclides (e.g. Stuiver and Braziunas 1998; Vonmoos, Beer, and Muscheler 2006; Usoskin et al. 2016; Usoskin 2017; Vecchio et al. 2017; Petrie, Criscuoli, and Bertello 2021). Modeling these variations provides a key input for understanding the

[1] https://lasp.colorado.edu/sorce/files/2020/04/SORCE_SOLSTICE_Release_Notes_for_Version_17.pdf.

global dynamics of the Earth's climate system (see, e.g., Lockwood 2012; Solanki, Krivova, and Haigh 2013; Bordi, Berrilli, and Pietropaolo 2015; Matthes et al. 2017; Liu et al. 2023).

In this article, we reconstruct four UV spectral bands (100 – 243 nm, 243 – 308 nm, FUV and MUV) over the past millennium using the same approach adopted in Penza et al. (2022) and Penza et al. (2024), where the method was applied to reconstruct the TSI. The applicability of this approach to spectral UV irradiance, beyond its original use for TSI reconstruction, is supported by several studies (e.g. Krivova et al. 2003; Wenzler et al. 2006; Ball et al. 2011; Fontenla et al. 2011; Lean et al. 2020). These suggest that solar irradiance variability across all wavelengths is entirely driven by the evolution of the magnetic field at the solar surface, which can be represented by the combined contributions of a limited set of magnetic structures, such as sunspots, faculae, and the network. Moreover, in the UV range, it is well established that irradiance variability is predominantly driven by bright features such as faculae and network regions, while the contribution from sunspots is almost negligible. This approach has also enabled the reconstruction of specific UV proxies, such as the Mg II index (e.g. Lean et al. 1997; Criscuoli et al. 2018; Berrilli et al. 2020; Sowmya et al. 2025).

Specifically, we employ the same composite of active region coverages (Chatzistergos et al. 2020; Mandal et al. 2020) and the same composite of open solar flux F_0, with the latter serving as a proxy for tracking long-term changes on time scales larger than the 22-year solar magnetic cycle. The composite of F_0 for the period 971–1899 C.E. is derived from the reconstruction by Usoskin et al. (2021), which is based specifically on the cosmogenic isotope ^{14}C. The extension to the present (1900 – 2020 C.E.) is obtained using an empirical relation between F_0 and the solar modulation potential ϕ, given by Muscheler et al. (2007) for 1513 – 1949 C.E. and by Usoskin (2017) for 1950 – 2025 C.E. The reconstruction of F_0 for the post-1900 period has been validated by comparison with observational data from Owens et al. (2017).

2. Reconstruction of UV Bands over the Solar Cycle

2.1. UV Data and Selected Bands

The UV data used in this work to parameterize the reconstruction are from the SSI3 (SSI, solar spectral irradiance) composite by Woods and DeLand (2021). We refer to the website of the Laboratory for Atmospheric and Space Physics (LASP) [2] for a detailed description of the instrumentation and the composite construction.

In particular, we consider UV data for the period 1980 – 2020 C.E. and in the wavelength range 100 – 310 nm, within which we identify four specific bands of interest:

- FUV (far ultraviolet): 115 – 180 nm;
- MUV (middle ultraviolet): 180 – 310 nm;
- UV_1: 100 – 243 nm;
- UV_2: 243 – 308 nm.

An example of an SSI3 composite spectrum is shown in Figure 1, where the four bands mentioned above are highlighted using different colors.

The FUV and MUV bands allow the calculation of the spectral color index, defined as:

$$\mathrm{FUV} - \mathrm{MUV} = -2.5 \log \frac{F_{fuv}}{F_{muv}} + Z_{fuv} + Z_{muv} \tag{1}$$

[2] https://lasp.colorado.edu/lisird/data/lasp_gsfc_composite_ssi.

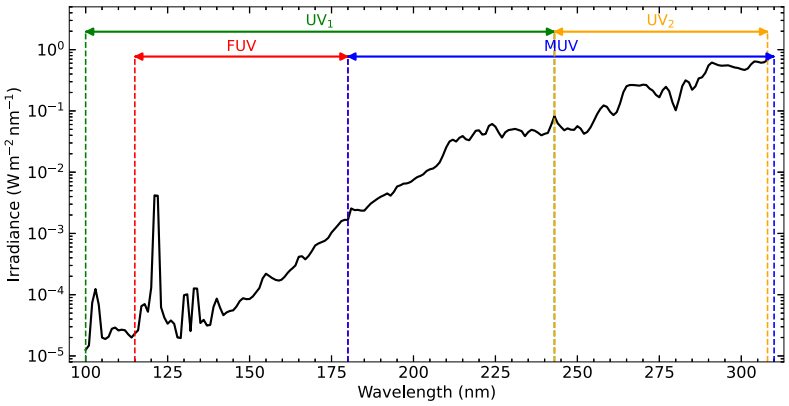

Figure 1 An example of a SSI3 composite spectrum, in logarithmic scale, from 100 nm to 310 nm with different bands highlighted by different colors.

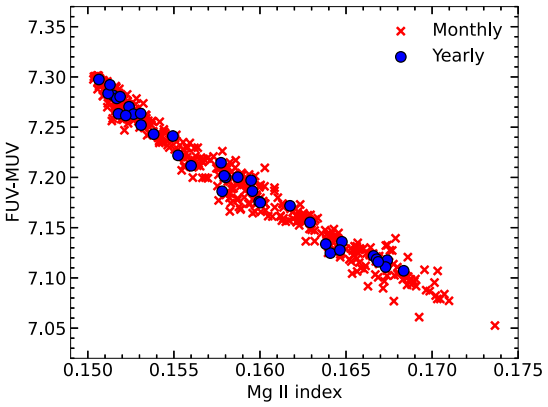

Figure 2 The correlation between FUV-MUV color and the Bremen Mg II index is shown for monthly values (red crosses) and for yearly averaged data (blue points) for the period 1980 – 2016. The Pearson's coefficient is r =-0.985 for monthly values and r =-0.989 for yearly values.

where F_{fuv} and F_{muv} are the fluxes integrated in the corresponding bands. In this work, the zero-point magnitudes, Z_{fuv} and Z_{muv}, are arbitrarily set to zero. This applies a constant vertical shift to all magnitude values but does not affect the subsequent results.

This quantity can be used to characterize the UV emission and is strongly correlated with the Mg II index (Lovric et al. 2017; Criscuoli et al. 2018). The UV_1 and UV_2 bands are selected due to their role in the atmospheric ozone cycle: the radiation in the UV_1 range is primarily responsible for the photodissociation of molecular oxygen (O_2), initiating ozone (O_3) production, while UV_2 radiation contributes, together with UV_1, to both ozone formation and destruction through photodissociation of ozone itself.

The correlation of the FUV-MUV color index with the Mg II Bremen composite index[3] is shown in Figure 2, where a strong anti-correlation is clearly visible, with a Pearson's correlation coefficient of $r = -0.989$. The best-fit linear regression of the correlation is in the form

$$\text{FUV} - \text{MUV} = \alpha\, \text{Mg II} + \beta \tag{2}$$

[3] https://lasp.colorado.edu/lisird/data/bremen_composite_mgii.

where in the case of monthly values $\alpha = -10.63 \pm 0.09$ and $\beta = 8.89 \pm 0.01$, while for yearly values $\alpha = -10.6 \pm 0.3$ and $\beta = 8.88 \pm 0.04$.

2.2. Reconstruction of UV Bands along the Last Four Cycles

Solar irradiance is reconstructed as the sum of contributions from various solar surface components, each weighted by its respective coverage area:

$$F(\lambda, t) = \sum_j \alpha_j(t) F_j(\lambda), \tag{3}$$

where $F_j(\lambda)$ is the flux at wavelength λ from the j^{th} feature (assumed time-independent), and $\alpha_j(t)$ is the corresponding coverage. The number and type of these components depend on the spectral band under consideration. Given that UV irradiance variability is primarily dominated by bright features, we can expand Equation 3 as follows:

$$F(\lambda_{UV}, t) = \alpha_f(t) F_f(\lambda_{UV}) + \alpha_n(t) F_n(\lambda_{UV}) + (1 - \alpha_f(t) - \alpha_n(t)) F_q(\lambda_{UV}) \tag{4}$$

where the subscripts f, n, and q indicate facular, network, and quiet solar contributions, respectively. Then, the relative variation of the flux at a given wavelength has a very simple form:

$$\delta F(\lambda_{UV}, t) \equiv \frac{F(\lambda_{UV}, t) - F_q(\lambda_{UV})}{F_q(\lambda_{UV})} = \alpha_f(t) \delta_f^{UV} + \alpha_n(t) \delta_n^{UV} \tag{5}$$

where δ_f^{UV} and δ_n^{UV} are the contrasts relative to the quiet Sun in the UV band of interest.

As shown in Penza et al. (2022) and Penza et al. (2024), we adopt a linear relation between $\alpha_f(t)$ and $\alpha_n(t)$ (e.g. Criscuoli 2016; Criscuoli et al. 2018; Devi et al. 2021; Ermolli, Giorgi, and Chatzistergos 2022):

$$\alpha_n(t) = A_n + B_n \alpha_f(t). \tag{6}$$

This relationship should be regarded as a simplification of the actual and complex correlation between magnetic structures. Anyway, the existence of a clear correlation between network and plage is well illustrated in Figure 13 of Ermolli, Giorgi, and Chatzistergos (2022). Moreover, Figure 4 of Criscuoli (2016) shows that pixels with different magnetic field strengths scale linearly with the sunspot number, implying that pixels with different magnetic field strengths should also scale linearly with each other. That allows us to rewrite Equation 5 as:

$$\delta F(\lambda_{UV}, t) = \alpha_f(t) \delta_{fn}^{UV} + C_n^{UV} \tag{7}$$

where $\delta_{fn} \equiv \delta_f^{UV} + B_n \delta_n^{UV}$ is the mixed facular and network contribution, while $C_n^{UV} \equiv A_n \delta_n^{UV}$ represents the value of the network contrast weighted by the corresponding fractional area at the solar minimum. As in Penza et al. (2024), we use the plage coverage composite provided by Chatzistergos et al. (2020)[4] for this reconstruction. In order to obtain an estimation of the parameters δ_{fn} and C_n^{UV}, SSI3 observations of Cycle 22 and 23 were separately fit using Equation 7. The mean of two best-fits gives the values reported in Table 1.

[4]available at https://www2.mps.mpg.de/projects/sun-climate/data.html.

Table 1 Values of the parameters of Equation 7, obtained by best fitting to SSI3 data separately for Solar Cycles 22 and 23.

Band	δ_{fn}	C_n
FUV	4.82 ± 0.05	0.005 ± 0.001
MUV	0.17 ± 0.1	0.004 ± 0.001
UV_1	0.64 ± 0.01	0.004 ± 0.001
UV_2	0.17 ± 0.01	0.004 ± 0.001

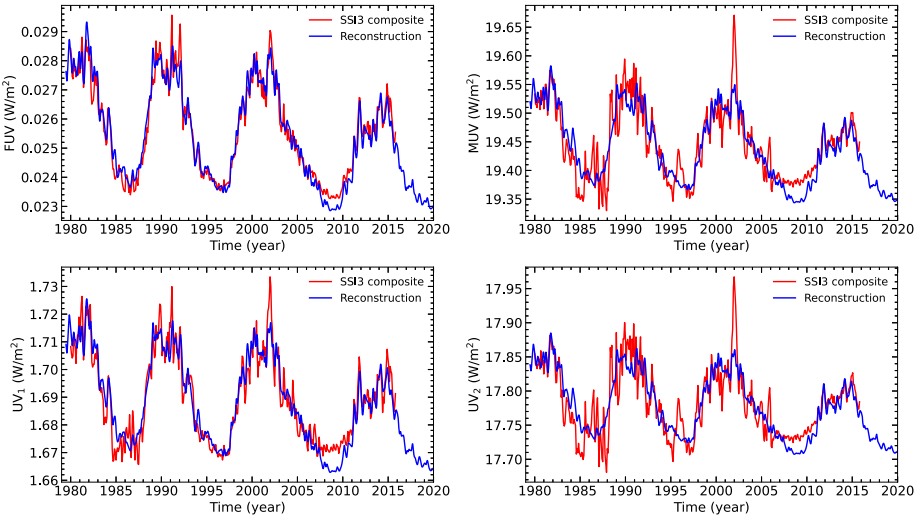

Figure 3 Comparison of the monthly averages of the reconstruction (blue line) and the SSI3 composite data (red line) for the four UV bands: FUV (top-left), MUV (top-right), UV_1 (bottom-left), and UV_2 (bottom-right).

Although we have imposed no constraints on the model, these values are compatible with those reported in literature (Lean 1997; Fontenla et al. 1999). We show the different reconstructions, obtained with the approach described above, in Figure 3, where we compare them with the corresponding SSI3 composite data. The figure highlights that the longer wavelength data exhibit an anomalous increase in irradiance around 2002 (the second peak of Solar Cycle 23), a feature absent at shorter wavelengths (FUV). We suppose that this behavior is not physical, but rather the result of an instrumentation artifact. However, we chose to retain these outlier data, considering that their short duration does not affect the integrity of our reconstruction.

3. Reconstruction of UV Bands along the Last Millenium

3.1. Plage Coverage Reconstruction

To reconstruct the UV spectral bands over the past millennium, we use the plage coverage time series previously reconstructed by Penza et al. (2024). In the following, we summarize the key aspects of that reconstruction.

1. *Definition of a Parametric Functional Form of the Cycle*
   We reproduce sunspot coverage of the k cycle by using the functional form suggested by Volobuev (2009):

$$x_k(t) = \left(\frac{t - T0_k}{Ts_k}\right)^2 \exp\left[-\left(\frac{t - T0_k}{Td_k}\right)^2\right] \quad T0_k < t < T0_k + \tau_k \tag{8}$$

   In reality, there is a relationship between the two free parameters Ts_k and Td_k. This relation reflects the well-known Waldmeier rule, which states that solar cycles with shorter rise times (i.e., smaller Td_k) tend to have larger amplitudes (corresponding to smaller Ts_k). Lastly, $T0_k$ is the start time and τ_k is the duration of cycle k. Using the data composite (1874 – 2023 E.C.) from Mandal et al. (2020), we obtain the values of the parameters Td_k and Ts_k for the thirteen solar cycles spanning Cycles 12 to 24.
2. *Determination of a Correlation between Cycle Parameters and the Open Solar Flux*
   We use the same open flux composite F_o used in Penza et al. 2024, constructed through inter-calibration of the following datasets: open solar flux F_o by Usoskin et al. (2021) for the period 971 – 1899 E.C., solar modulation potential by Muscheler et al. (2007) for the period 1513 – 2001 E.C., and solar modulation potential from a neutron monitor by Usoskin (2017) for the period 1950 – 2020 E.C.
   The relation identified in Penza et al. (2024) establishes the following connection between the 11-year cycle-averaged F_o values ($\overline{F_o}$) and the parameter $P_k \equiv (Td_k/Ts_k)^2$, which is proportional to the analytical integral of Equation 8:

$$P_k = (0.002 \pm 0.001)\overline{F_o} + (-0.004 \pm 0.003) \tag{9}$$

   Equation 9 allows us to obtain the values of P_k, then of Td_k and Ts_k, and to reconstruct the sunspot area from 971 E.C. This preliminary reconstruction of sunspot areas is necessary in order to reconstruct the plage coverage. It is needed because the most recent composite indicates a non-zero plage coverage during solar minima, making functional forms like ours unsuitable, as they are by definition zero at the beginning of each cycle.
3. *Reconstruction of Plage Coverage*
   The reconstruction of the plage coverage is derived from the well-established power-law relationship between plage and sunspot coverages (Chatzistergos et al. 2022; Penza et al. 2024). In particular, in Penza et al. (2024) the authors find the following relation between the monthly averages of sunspot (Mandal et al. 2020) and plage (Chatzistergos et al. 2020) area coverages within the common time range 1903 – 2023 C.E.:

$$\alpha_f = (1.3 \pm 0.1)\alpha_s^{(0.61 \pm 0.02)} + (0.0042 \pm 0.0005) \tag{10}$$

   The final reconstruction of plage coverage from 971 E.C. to the present is presented in Figure 4.

3.2. UV Band Reconstruction

In order to reconstruct the UV bands over the last millenium, we use Equation 7, with the contrast parameters obtained by the fits along the single cycles. Nevertheless, it is necessary to account for the long-term variations affecting the open magnetic field, that we associate with the quiet network component. Accordingly, the equation can be rewritten as follows:

$$\delta F(t) = C_n\,[1 + F_{LT}(t)]\,N_{norm} + \alpha_f(t)\delta_{fn} \tag{11}$$

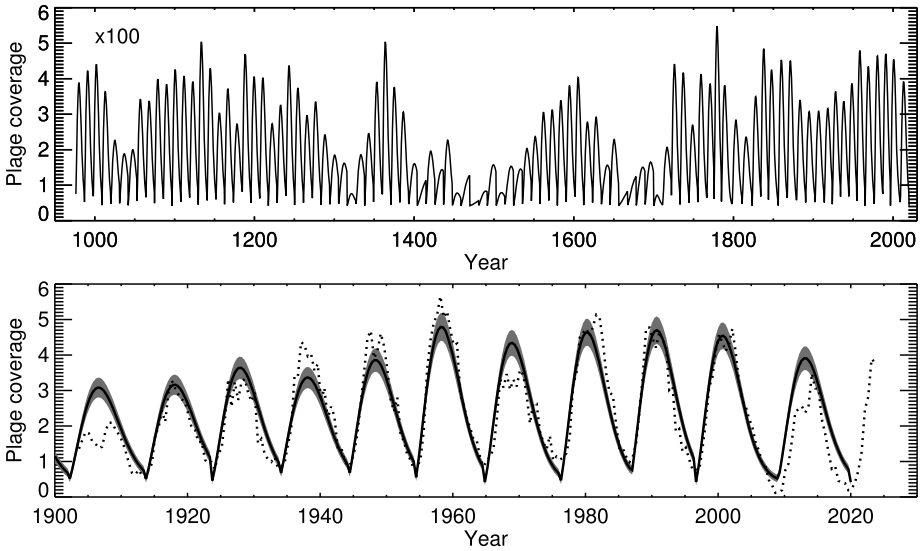

Figure 4 Top panel: Reconstruction of plage area coverage from 971 CE to the present. Bottom Panel: The reconstructed time series (solid curve) and its uncertainty range (grey region) are shown from 1900 to the present. The actual measured monthly plage area coverage by Chatzistergos et al. (2020) is shown as a dotted line.

Table 2 Values of the parameters of Equation 11, obtained by best fitting to the full SSI3 dataset over the period 1980 – 2015.

Band	N_{norm}	F_q (Wm^{-2})
FUV	6.34 ± 0.01	0.020 ± 0.001
MUV	0.97 ± 0.01	31.10 ± 0.01
UV_1	2.16 ± 0.01	1.63 ± 0.01
UV_2	0.91 ± 0.01	17.50 ± 0.01

where $F_{LT}(t)$ is a normalized long-term modulation function and N_{norm} is a normalization parameter. $F_{LT}(t)$ is the same function computed in Penza et al. (2024). It is derived by decomposing the F_o composite into Intrinsic Mode Functions (IMFs) using Empirical Mode Decomposition (EMD) (Huang et al. 1998), and then selecting only those components with characteristic timescales longer than 22 years, along with the monotonic trend. In other words, this process removes the variability on timescales shorter than 22 years from F_o, which is already captured in the temporal evolution of the plage component.

For the final reconstruction, the two free parameters N_{norm} and F_q are obtained by the four best fit over the SSI3 composite (one for each wavelength band), by considering the whole period 1980 – 2020. The values of the free parameters are reported in Table 2, while the resulting final reconstructions of the four UV bands are shown in Figure 5, which also includes the reconstruction of the FUV–MUV color index.

4. Discussion and Conclusions

In this work, we present a reconstruction of solar UV variability over the last millennium, covering the period from 971 to 2020 CE. The methodology used is the same as in Penza

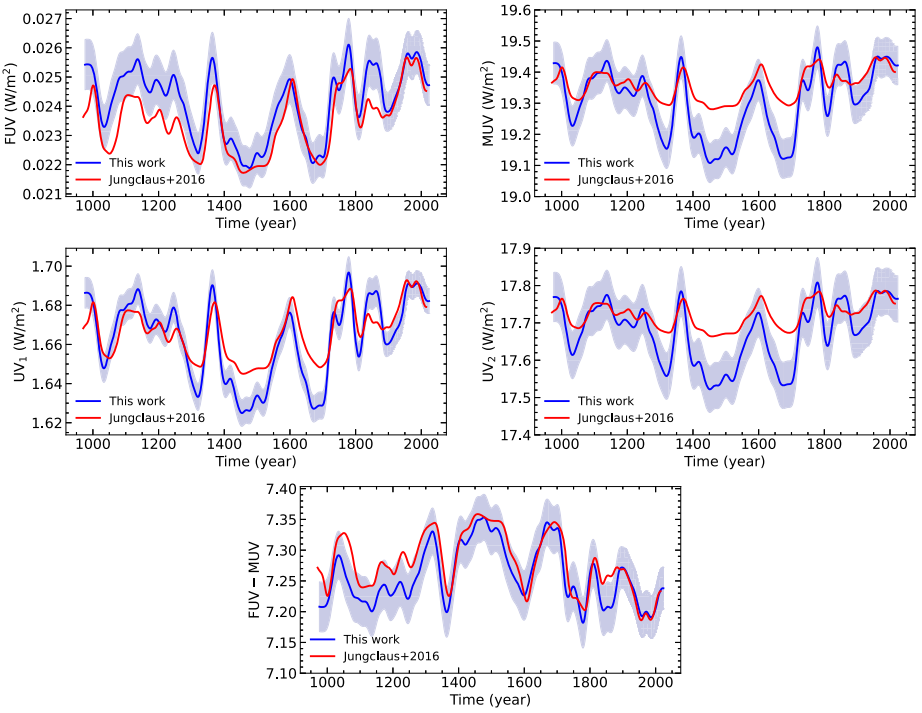

Figure 5 Smoothed 22-year reconstructions from 971 CE to the present, obtained in this work (blue line), along with their uncertainty ranges (shaded blue regions). This uncertainty arises from the propagation of errors in the plage coverage and in the coefficients in Table 2. The red lines represent the corresponding reconstructions from Jungclaus et al. (2016). The five panels show: FUV (top-left), MUV (top-right), UV_1 (middle-left), UV_2 (middle-right), and the color index FUV-MUV (bottom).

et al. (2024), the reconstruction is based on plage coverage data from Chatzistergos et al. (2020), and the open magnetic field proxy from Usoskin et al. (2021). Using this approach, we reconstruct four UV bands: FUV (115 – 180 nm), MUV (180 – 310 nm), UV_1 (100 – 243 nm), and UV_2 (243 – 308 nm). In addition to these four bands, we also reconstruct the FUV–MUV color index.

We have confirmed that including the long-term modulation factor F_{LT} in the reconstruction improves its agreement with the SSI3 composite data over the 1980 – 2015 period, as clearly shown in Figure 6. The figure presents results for the FUV and MUV bands, while similar improvements are also observed for the UV_1 and UV_2 bands (not shown). In particular, the long-term modulation factor plays a more significant role for the longer-wavelength bands (i.e., MUV) than for the shorter ones. The reconstruction includes two bands, here indicated with UV_1 and UV_2, which are directly associated with the photochemical production and destruction of ozone in the Earth's atmosphere.

The final reconstructed time series for each band are presented in Figure 5. For the FUV and UV_1 bands, our reconstruction closely resembles that of Jungclaus et al. (2016), which is based on the ^{14}C record and Spectral And Total Irradiance REconstructions (SATIRE) models. Conversely, significant deviations are observed in the longer-wavelength bands (MUV and UV2).

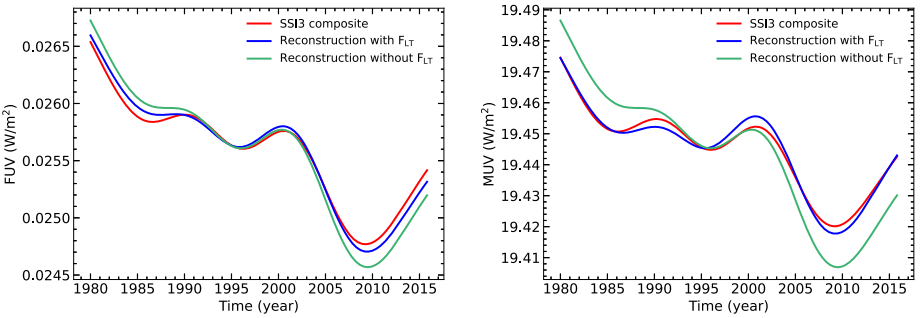

Figure 6 Comparison between the reconstruction with (blue) and without (green) the long-term modulation F_{LT} and the SSI3 composite (red), for the FUV (left panel) and MUV (right panel) bands. All data are smoothed over 11 years.

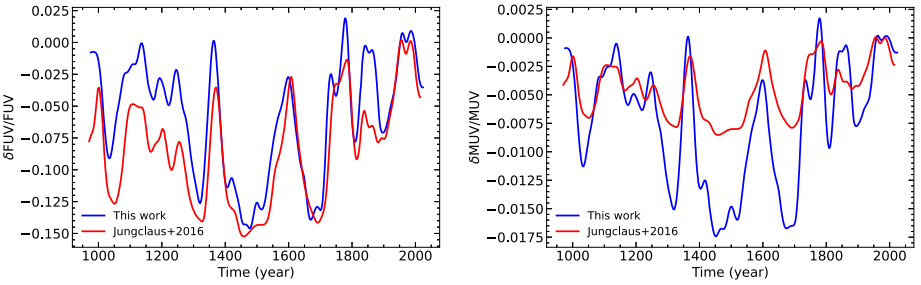

Figure 7 Comparison of irradiance variations relative to the present in the FUV (left) and MUV (right) bands between our reconstruction and the SATIRE model (Jungclaus et al. 2016). The present-day value is defined as the average of the SSI3 data from 1980 to 2015.

Both our reconstruction and that of Jungclaus et al. (2016) estimate a variation of approximately 15% in the FUV band during the Spörer and Maunder minima relative to the present-day level, defined as the average value of the SSI3 data from 1980 to 2015. However, the variation in the MUV band is considerably smaller, with the SATIRE model estimating only about 0.7%, whereas our reconstruction exceeds 1.6% (Figure 7). This discrepancy likely arises from the modulation factor we introduced to the quiet-network component, which, as shown in Figure 6, has a stronger influence on the longer wavelength bands than on the shorter ones.

The reconstructed FUV and MUV bands also allow for the calculation of the FUV–MUV color index, which can be used to characterize stellar UV emission (Schindhelm et al. 2015; Calabrò et al. 2021) and is strongly correlated with the Mg II index (Lovric et al. 2017; Criscuoli et al. 2018). Because the FUV-MUV modulation is mainly driven by variations in the FUV, our reconstruction does not deviate significantly from the SATIRE model one. The computation of the FUV-MUV color index places this study within a broader stellar context. Studying UV irradiance variations in stars other than the Sun is a topic of great interest in stellar astrophysics (Lubin, Melis, and Tytler 2018; Namekata et al. 2023). In fact, ultraviolet radiation plays a key role in shaping exoplanetary atmospheres through photochemical processes and atmospheric erosion, thereby influencing climate and surface conditions critical to habitability (e.g. Segura et al. 2005; Reda et al. 2022; Spinelli et al. 2023; Li et al. 2024). By characterizing solar UV variability over long timescales in relation to broad lev-

els of solar activity, we gain valuable insights that can be extended to the study of stellar environments and their impact on planetary systems conditions.

Acknowledgments The National Solar Observatory is operated by the Association of Universities for Research in Astronomy, Inc. (AURA), under cooperative agreement with the National Science Foundation. L.B. and S.C. are members of the international team on Reconstructing Solar and Heliospheric Magnetic Field Evolution Over the Past Century supported by the International Space Science Institute (ISSI), Bern, Switzerland. L.L. is supported by the Joint Research PhD Program in "Astronomy, Astrophysics and Space Science" between the University of Rome "Tor Vergata", the University of Rome "La Sapienza" and INAF. The authors acknowledge the Space It Up project funded by the Italian Space Agency, ASI, and the Ministry of University and Research, MUR, under contract n. 2024-5-E.0 – CUP n. I53D24000060005. "Realizzazione di un'Infrastruttura HW e SW (IHS) presso il CGS/Matera (CUP F83C22002460005), in attuazione del Piano Operativo del sub-investimento M1C2.I4.4 'In-Orbit Economy – SST—FlyEye' del PNRR-FC".

Author Contributions V.P. and S.C. worked on the UV reconstruction. L.L and F.B. worked on the relationship between UV and the Earth's atmosphere. L.B. worked on the statistical analysis and figures. M.C. worked on EMD analysis and calibration. S.U. worked on cosmogenic isotopes data and open flux connection. V.P and R.R. wrote the initial draft. All authors reviewed the manuscript and analysis.

Funding Information Open access funding provided by Università degli Studi di Roma Tor Vergata within the CRUI-CARE Agreement.

Data Availability No datasets were generated or analyzed during the current study.

Declarations

Competing Interests The authors declare no competing interests.

References

Ball, W.T., Unruh, Y.C., Krivova, N.A., Solanki, S., Harder, J.W.: 2011, Solar irradiance variability: a six-year comparison between SORCE observations and the SATIRE model. *Astron. Astrophys.* **530**, A71. DOI. ADS.

Berrilli, F., Ermolli, I., Florio, A., Pietropaolo, E.: 1999, Average properties and temporal variations of the geometry of solar network cells. *Astron. Astrophys.* **344**, 965. ADS.

Berrilli, F., Criscuoli, S., Penza, V., Lovric, M.: 2020, Long-term (1749 – 2015) variations of solar UV spectral indices. *Sol. Phys.* **295**, 38. DOI. ADS.

Bigazzi, A., Cauli, C., Berrilli, F.: 2020, Lower-thermosphere response to solar activity: an empirical-mode-decomposition analysis of GOCE 2009 – 2012 data. *Ann. Geophys.* **38**, 789. DOI. ADS.

Bordi, I., Berrilli, F., Pietropaolo, E.: 2015, Long-term response of stratospheric ozone and temperature to solar variability. *Ann. Geophys.* **33**, 267. DOI. ADS.

Calabrò, A., Castellano, M., Pentericci, L., Fontanot, F., Menci, N., Cullen, F., McLure, R., Bolzonella, M., Cimatti, A., Marchi, F., Talia, M., Amorín, R., Cresci, G., De Lucia, G., Fynbo, J., Fontana, A., Franco, M., Hathi, N.P., Hibon, P., Hirschmann, M., Mannucci, F., Santini, P., Saxena, A., Schaerer, D., Xie, L., Zamorani, G.: 2021, The VANDELS survey: the relation between the UV continuum slope and stellar metallicity in star-forming galaxies at z $\sim$ 3. *Astron. Astrophys.* **646**(A39). DOI. ADS.

Cebula, R.P., Park, H., Heath, D.F.: 1988, Characterization of the Nimbus-7 SBUV radiometer for the long-term monitoring of stratospheric ozone. *J. Atmos. Ocean. Technol.* **5**, 215. DOI. ADS.

Chapman, S.: 1930, A theory of upper atmosphere ozone. *Mem. R. Meteorol. Soc.* **3**, 103.
Chatzistergos, T., Ermolli, I., Krivova, N.A., Solanki, S.K., Banerjee, D., Barata, T., Belik, M., Gaifera, R., Garcia, A., Hanaoka, Y., Hedge, M., Klimes, J., Korokhin, V.V., Lourenço, A., Malherbe, J., Marchenko, G., Peixinho, N., Sakurai, T., Tlatov, A.: 2020, Analysis of full-disc Ca II K spectroheliograms. III. Plage area composite series covering 1892 – 2019. *Astron. Astrophys.* **639**, 22. DOI.
Chatzistergos, T., Ermolli, I., Krivova, N.A., Barata, T., Carvalho, S., Malherbe, J.: 2022, Scrutinising the relationship between plage areas and sunspot areas and numbers. *Astron. Astrophys.* **667**, 21. DOI.
Criscuoli, S.: 2016, Angular dependence of the facular-sunspot coverage relation as derived by MDI magnetograms. *Sol. Phys.* **291**, 1957. DOI. ADS.
Criscuoli, S.: 2019, Effects of continuum fudging on non-LTE synthesis of stellar spectra. I. Effects on estimates of UV continua and solar spectral irradiance variability. *Astrophys. J.* **872**, 52. DOI. ADS.
Criscuoli, S., Penza, V., Lovric, M., Berrilli, F.: 2018, The correlation of synthetic UV color versus Mg II index along the solar cycle. *Astrophys. J.* **865**, 22. DOI. ADS.
Criscuoli, S., Marchenko, S., DeLand, M., Choudhary, D., Kopp, G.: 2023, Understanding sun-as-a-star variability of solar Balmer lines. *Astrophys. J.* **951**, 151. DOI. ADS.
Devi, P., Singh, J., Chandra, R., Priyal, M., Joshi, R.: 2021, Variation of chromospheric features as a function of latitude and time using Ca-K spectroheliograms for solar cycles 15 – 23: implications for meridional flow. *Sol. Phys.* **296**, 49. DOI. ADS.
Ermolli, I., Berrilli, F., Florio, A.: 2003, A measure of the network radiative properties over the solar activity cycle. *Astron. Astrophys.* **412**, 857. DOI. ADS.
Ermolli, I., Giorgi, F., Chatzistergos, T.: 2022, Rome precision solar photometric telescope: precision solar full-disk photometry during solar cycles 23 – 25. *Front. Astron. Space Sci.* **9**, 352. DOI. ADS.
Fontenla, J., White, O.R., Fox, P.A., Avrett, E.H., Kurucz, R.L.: 1999, Calculation of solar irradiances. I. Synthesis of the solar spectrum. *Astrophys. J.* **518**, 480. DOI. ADS.
Fontenla, J.M., Harder, J., Livingston, W., Snow, M., Woods, T.: 2011, High-resolution solar spectral irradiance from extreme ultraviolet to far infrared. *J. Geophys. Res., Atmos.* **116**, D20108. DOI. ADS.
Fröhlich, C., Lean, J.: 2004, Solar radiative output and its variability: evidence and mechanisms. *Astron. Astrophys. Rev.* **12**, 273. DOI. ADS.
Galuzzo, D., Cagnazzo, C., Berrilli, F., Fierli, F., Giovannelli, L.: 2021, Three-dimensional climate simulations for the detectability of Proxima Centauri B. *Astrophys. J.* **909**, 191. DOI. ADS.
Haigh, J.D.: 2007, The Sun and the Earth's climate. *Living Rev. Sol. Phys.* **4**, 2. DOI. ADS.
Huang, N.E., Shen, Z., Long, S.R., Wu, M.C., Shih, H.H., Zheng, Q., Yen, N.-C., Tung, C.C., Liu, H.H.: 1998, The empirical mode decomposition and the Hilbert spectrum for nonlinear and non-stationary time series analysis. *Proc. R. Soc. Lond. Ser. A* **454**, 903. DOI. ADS.
Jungclaus, J.H., Bard, E., Baroni, M., Braconnot, P., Cao, J., Chini, L.P., Egorova, T., Evans, M., Fidel González-Rouco, J., Goosse, H., Hurtt, G.C., Joos, F., Kaplan, J.O., Khodri, M., Klein Goldewijk, K., Krivova, N., LeGrande, A.N., Lorenz, S.J., Luterbacher, J., Man, W., Maycock, A.C., Meinshausen, M., Moberg, A., Muscheler, R., Nehrbass-Ahles, C., Otto-Bliesner, B.I., Phipps, S.J., Pongratz, J., Rozanov, E., Schmidt, G.A., Schmidt, H., Schmutz, W., Schurer, A., Shapiro, A.I., Sigl, M., Smerdon, J.E., Solanki, S.K., Timmreck, C., Toohey, M., Usoskin, I.G., Wagner, S., Wu, C.-J., Leng Yeo, K., Zanchettin, D., Zhang, Q., Zorita, E.: 2016, The PMIP4 contribution to CMIP6 – part 3: the last millennium, scientific objective, and experimental design for the PMIP4 past1000 simulations. *Geosci. Model Dev.* **10**, 4005. DOI. ADS.
Kakuwa, J., Satoru, U.: 2022, Investigation of the long-term variation of solar Ca II K intensity. II. Reconstruction of solar UV irradiance. *Astron. J.* **928**, 97. DOI. https://iopscience.iop.org/article/10.3847/1538-4357/ac5963/pdf.
Kopp, G., Krivova, N., Wu, C.J., Lean, J.: 2016, The impact of the revised sunspot record on solar irradiance reconstructions. *Sol. Phys.* **291**, 2951. DOI. ADS.
Krivova, N.A., Solanki, S.K., Fligge, M., Unruh, Y.C.: 2003, Reconstruction of solar irradiance variations in cycle 23: is solar surface magnetism the cause? *Astron. Astrophys.* **399**, L1. DOI. ADS.
Lean, J.: 1997, The Sun's variable radiation and its relevance for Earth. *Annu. Rev. Astron. Astrophys.* **35**, 33. DOI. ADS.
Lean, J.L., Rottman, G.J., Kyle, H.L., Woods, T.N., Hickey, J.R., Puga, L.C.: 1997, Detection and parameterization of variations in solar mid- and near-ultraviolet radiation (200 – 400 nm). *J. Geophys. Res.* **102**, 29939. DOI. ADS.
Lean, J.L., Coddington, O., Marchenko, S.V., Machol, J., DeLand, M.T., Kopp, G.: 2020, Solar irradiance variability: modeling the measurements. *Earth Space Sci.* **7**, 00645. DOI. ADS.
Li, X., Wang, S., Han, H., Yang, H., Zheng, C., Huang, Y., Liu, J.: 2024, Ultraviolet and chromospheric activity and habitability of M stars. *Astrophys. J.* **966**, 69. DOI. ADS.
Lilensten, J., Tourpali, K.: 2015, Direct impact of solar irradiance variability. In: *Earth's Climate Response to a Changing Sun*, EDP Science, 229. Chapter 4.1. ISBN 978–2–7598–1733–7. DOI.

Linsky, J.: 2014, The radiation environment of exoplanet atmospheres. *Challenges* **5**, 351. DOI. ADS.
Liu, H.-L., Rempel, M., Danabasoglu, G., Solomon, S.C., McInerney, J.M.: 2023, Climate responses under an extreme quiet Sun scenario. *J. Geophys. Res., Atmos.* **128**, e2022JD037626. DOI. ADS.
Lockwood, M.: 2012, Solar influence on global and regional climates. *Surv. Geophys.* **33**, 503. DOI.
Lovric, M., Tosone, F., Pietropaolo, E., Del Moro, D., Giovannelli, L., Cagnazzo, C., Berrilli, F.: 2017, The dependence of the [FUV-MUV] colour on solar cycle. *J. Space Weather Space Clim.* **7**, A6. DOI. ADS.
Lubin, D., Melis, C., Tytler, D.: 2018, Ultraviolet flux decrease under a grand minimum from IUE short-wavelength observation of solar analogs. *Astrophys. J. Lett.* **852**, L4. DOI. ADS.
Mandal, S., Krivova, N.A., Solanki, S.K., Sinha, N., Banerjee, D.: 2020, Sunspot area catalog revisited: daily cross-calibrated areas since 1874. *Astron. Astrophys.* **640**, A78. DOI. ADS.
Marchenko, S.V., Ludewig, A., Criscuoli, S., Al Moulla, K., Choudhary, D.P., DeLand, M.T., Kopp, G., Loots, E., van der Plas, E., Veefkind, P.: 2024, Sun-as-a-star spectral line variability in the 300 – 2390 nm wavelength range. *Astrophys. J.* **977**, 33. DOI. ADS.
Matthes, K., Funke, B., Andersson, M.E., Barnard, L., Beer, J., Charbonneau, P., Clilverd, M.A., Dudok de Wit, T., Haberreiter, M., Hendry, A., Jackman, C.H., Kretzschmar, M., Kruschke, T., Kunze, M., Langematz, U., Marsh, D.R., Maycock, A.C., Misios, S., Rodger, C.J., Scaife, A.A., Seppälä, A., Shangguan, M., Sinnhuber, M., Tourpali, K., Usoskin, I., van de Kamp, M., Verronen, P.T., Versick, S.: 2017, Solar forcing for CMIP6 (v3.2). *Geosci. Model Dev.* **10**, 2247. DOI. ADS.
McClintock, W.E., Snow, M., Woods, T.N.: 2005, Solar-stellar irradiance comparison experiment II (SOLSTICE II): pre-launch and on-orbit calibrations. *Sol. Phys.* **230**, 259. DOI. ADS.
Muscheler, R., Joos, F., Beer, J., Müller, S.A., Vonmoos, M., Snowball, I.: 2007, Solar activity during the last 1000 yr inferred from radionuclide records. *Quat. Sci. Rev.* **26**, 82. DOI. ADS.
Namekata, K., Toriumi, S., Airapetian, V.S., Shoda, M., Watanabe, K., Notsu, Y.: 2023, Reconstructing the XUV spectra of active sun-like stars using solar scaling relations with magnetic flux. *Astrophys. J.* **945**, 147. DOI. ADS.
Neupert, W.M.: 1965, Intensity variations in the solar extreme ultraviolet spectrum observed by OSO-1. *Ann. Astrophys.* **28**, 446. ADS.
Owens, M.J., Lockwood, M., Riley, P., Linker, J.: 2017, Sunward strahl: a method to unambiguously determine open solar flux from in situ spacecraft measurements using suprathermal electron data. *J. Geophys. Res. Space Phys.* **122**, 980. DOI.
Penza, V., Berrilli, F., Bertello, L., Cantoresi, M., Criscuoli, S., Giobbi, P.: 2022, Total solar irradiance during the last five centuries. *Astrophys. J.* **937**, 84. DOI.
Penza, V., Bertello, L., Cantoresi, M., Criscuoli, S., Lucaferri, L., Reda, R., Ulzega, S., Berrilli, F.: 2024, Reconstruction of the total solar irradiance during the last millennium. *Astrophys. J.* **976**, 11. DOI. ADS.
Petrie, G., Criscuoli, S., Bertello, L.: 2021, Solar magnetism and radiation. In: Raouafi, N.E., Vourlidas, A. (eds.) *Solar Physics and Solar Wind* **1**, 83. DOI. ADS.
Pienitz, R., Vincent, W.F.: 2000, Effect of climate change relative to ozone depletion on UV exposure in subarctic lakes. *Nature* **404**, 484. DOI. ADS.
Reda, R., Di Mauro, M.P., Giovannelli, L., Alberti, T., Berrilli, F., Corsaro, E.: 2022, A synergic strategy to characterize the habitability conditions of exoplanets hosted by solar-type stars. *Front. Astron. Space Sci.* **9**, 909268. DOI. ADS.
Reda, R., Giovannelli, L., Alberti, T., Berrilli, F., Bertello, L., Del Moro, D., Di Mauro, M.P., Giobbi, P., Penza, V.: 2023, The exoplanetary magnetosphere extension in Sun-like stars based on the solar wind-solar UV relation. *Mon. Not. R. Astron. Soc.* **519**, 6088. DOI. ADS.
Richard, E., Coddington, O., Harber, D., Chambliss, M., Penton, S., Brooks, K., Charbonneau, L., Peck, C., Béland, S., Pilewskie, P., Woods, T.: 2024, Advancements in solar spectral irradiance measurements by the TSIS-1 spectral irradiance monitor and its role for long-term data continuity. *J. Space Weather Space Clim.* **14**, 10. DOI. ADS.
Schindhelm, R., Stern, S.A., Gladstone, R., Zangari, A.: 2015, Pluto and Charon's UV spectra from IUE to new horizons. *Icarus* **246**, 206. DOI. ADS.
Segura, A., Kasting, J.F., Meadows, V., Cohen, M., Scalo, J., Crisp, D., Butler, R.A.H., Tinetti, G.: 2005, Biosignatures from Earth-like planets around M dwarfs. *Astrobiology* **5**, 706. DOI. ADS.
Solanki, S.K., Krivova, N.A., Haigh, J.D.: 2013, Solar irradiance variability and climate. *Annu. Rev. Astron. Astrophys.* **51**, 311. DOI.
Sowmya, K., Snow, M., Shapiro, A.I., Krivova, N.A., Chatzistergos, T., Solanki, S.K.: 2025, Solar variability in the Mg II h and k lines. *Astrophys. J.* **980**, 173. DOI. ADS.
Spinelli, R., Borsa, F., Ghirlanda, G., Ghisellini, G., Haardt, F.: 2023, The ultraviolet habitable zone of exoplanets. *Mon. Not. R. Astron. Soc.* **522**, 1411. DOI. ADS.
Steinegger, M., Brandt, P.N., Haupt, H.F.: 1996, Sunspot irradiance deficit, facular excess, and the energy balance of solar active regions. *Astron. Astrophys.* **310**, 635. ADS.

Stuiver, M., Braziunas, T.F.: 1998, Anthropogenic and solar components of hemispheric ^{14}C. *Geophys. Res. Lett.* **25**, 329. DOI. ADS.
Usoskin, I.G.: 2017, A history of solar activity over millennia. *Living Rev. Sol. Phys.* **14**, 3. DOI. ADS.
Usoskin, I.G., Gallet, Y., Lopes, F., Kovaltsov, G.A., Hulot, G.: 2016, Solar activity during the Holocene: the Hallstatt cycle and its consequence for grand minima and maxima. *Astron. Astrophys.* **587**, A150. DOI. https://www.aanda.org/articles/aa/pdf/2016/03/aa27295-15.pdf.
Usoskin, I.G., Solanki, S.K., Krivova, N.A., Hofer, B., Kovaltsov, G.A., Wacker, L., Brehm, N., Kromer, B.: 2021, Solar cyclic activity over the last millennium reconstructed from annual 14C data. *Astron. Astrophys.* **649**. DOI. ADS.
Vecchio, A., Lepreti, F., Laurenza, M., Alberti, T., Carbone, V.: 2017, Connection between solar activity cycles and grand minima generation. *Astron. Astrophys.* **599**, A58. DOI. ADS.
Volobuev, D.M.: 2009, The shape of the sunspot cycle: a one-parameter fit. *Sol. Phys.* **258**, 319. DOI.
Vonmoos, M., Beer, J., Muscheler, R.: 2006, Large variations in Holocene solar activity: constraints from ^{10}Be in the Greenland ice core project ice core. *J. Geophys. Res. Space Phys.* **111**, A10105. DOI. ADS.
Wenzler, T., Solanki, S.K., Krivova, N.A., Fröhlich, C.: 2006, Reconstruction of solar irradiance variations in cycles 21 – 23 based on surface magnetic fields. *Astron. Astrophys.* **460**, 583. DOI.
Woods, T.N., DeLand, M.T.: 2021, An improved solar spectral irradiance composite record. *Earth Space Sci.* **8**, e01740. DOI. ADS.

Authors and Affiliations

Raffaele Reda[1] · Valentina Penza[1] · Serena Criscuoli[2] · Luca Bertello[2] · Matteo Cantoresi[1] · Lorenza Lucaferri[1] · Simone Ulzega[3] · Francesco Berrilli[1]

✉ F. Berrilli
berrilli@roma2.infn.it

R. Reda
raffaele.reda@roma2.infn.it

V. Penza
penza@roma2.infn.it

S. Criscuoli
scriscuo@nso.edu

L. Bertello
luca@nso.edu

M. Cantoresi
matteo.cantoresi@roma2.infn.it

L. Lucaferri
lorenza.lucaferri@roma2.infn.it

S. Ulzega
ulzg@zhaw.ch

1 Dipartimento di Fisica, Università degli Studi di Roma Tor Vergata, Via della Ricerca Scientifica 1, Rome, 00133, Italy

2 National Solar Observatory, 3665 Discovery Dr., Boulder, CO 80303, USA

3 Institute of Computational Life Sciences, Zurich University of Applied Sciences (ZHAW), 8820 Wädenswil, Switzerland